

Contents lists available at ScienceDirect

Spectrochimica Acta Part A: Molecular and Biomolecular Spectroscopy

journal homepage: www.elsevier.com/locate/saa

A novel synthetic route for magnesium aluminate (MgAl_2O_4) nanoparticles using sol–gel auto combustion method and their photocatalytic properties



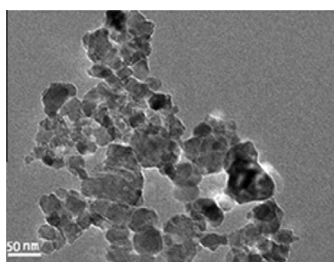
Mostafa Y. Nassar, Ibrahim S. Ahmed*, Ihab Samir

Faculty of Science, Chemistry Department, Benha University, Benha 13518, Egypt

HIGHLIGHTS

- Synthesis of MgAl_2O_4 nanoparticles using sol–gel auto combustion method.
- Effect of fuel type on MgAl_2O_4 nanoparticles was studied.
- Photocatalytic activity of MgAl_2O_4 using Reactive Red Me 4BL dye was investigated.

GRAPHICAL ABSTRACT



HR-TEM image of MgAl_2O_4 calcined at 800 °C prepared using oxalic acid fuel.

ARTICLE INFO

Article history:

Received 21 December 2013
Received in revised form 6 March 2014
Accepted 7 April 2014
Available online 20 April 2014

Keywords:

Inorganic compounds
Sol–gel auto combustion synthesis
Photocatalytic properties

ABSTRACT

In this paper a novel and inexpensive route for the preparation of spinel magnesium aluminate nanoparticles (MgAl_2O_4) is proposed. Magnesium aluminate photocatalyst was synthesized via sol–gel auto combustion method using oxalic acid, urea, and citric acid fuels at 350 °C. Subsequently, the burnt samples were calcined at different temperatures. The pure spinel MgAl_2O_4 with average crystallite size 27.7, 14.6 and 15.65 nm was obtained at 800 °C calcinations using the aforementioned fuels, respectively. The obtained samples were characterized by powder X-ray diffraction, Fourier transform infrared, UV–Vis spectroscopy, transmission electron microscope, scanning electron microscope. The photocatalytic activity of MgAl_2O_4 product was studied by performing the decomposition of Reactive Red Me 4BL dye under UV illumination or sunlight irradiation. The dye considerably photocatalytically degraded by 90.0% and 95.45% under UV and sunlight irradiation, respectively, within ca. 5 h with pseudo first order rate constants of 5.85×10^{-3} and $8.38 \times 10^{-3} \text{ min}^{-1}$, respectively.

© 2014 The Authors. Published by Elsevier B.V. This is an open access article under the CC BY-NC-ND license (<http://creativecommons.org/licenses/by-nc-nd/3.0/>).

Introduction

Global industrialization (such as textile, refineries, leather, paper, chemical, and plastic industries) has used different types of dyes resulted in the release of large amounts of toxic compounds

into environment [1,2]. Generally, 30–40% of these dyes remain in the waste waters. Additionally, presence of these dyes diminishes the photosynthesis and causes many serious health problems for humanity. To overcome these problems, the waste water from those industries must be treated before their discharge. Various physical and chemical methods have been used for color removal from waste waters. One of these methods is semiconductor photocatalysis and it has proven to be an effective in treating wastewater

* Corresponding author. Tel.: +20 1222408034.

E-mail address: isahmed2010@gmail.com (I.S. Ahmed).

pollution since it is an environmentally friendly, low-cost, and sustainable treatment methodology [3,4].

The search for low cost and efficient photocatalysts is still continuing. Some spinel-type oxides such as BaCr_2O_4 [5], NiFe_2O_4 [6], CaBi_2O_4 [7], ZnGa_2O_4 [8], CuGa_2O_4 [9], ZnFe_2O_4 [10] and CuAl_2O_4 [11–13] used as photocatalysts are semiconductor materials with narrow band high and these materials have been proven to be an efficient in the degradation of pollutants and/or the production of photocatalytic hydrogen. Many methods for preparation of nano-sized spinels have been reported such as co-precipitation [14], sol-gel [7,11], sonochemical [9], microemulsion [5] and solution combustion [13]. However, combustion method has many advantages compared to these methods as will be mentioned latter. Additionally, in the combustion technique, nitrates are used as oxidizers, and some organic compounds such as glycine, sucrose, sorbitol, and others are used as fuel. In which the heat released due to the combustion reaction between the oxidizers and the fuel which is exothermic cause can the preparation of the target nanomaterials [15–19].

Magnesium aluminate, MgAl_2O_4 , is a typical spinel material and it has also attracted growing interest in diverse applications such as refractory material, microwave dielectric and ceramic capacitor, humidity sensors, catalyst or catalyst support, and structural material in fusion reactors [20,21]. Plus, Magnesium aluminate has a low density (3.58 g/cm^3), high melting point ($2135 \text{ }^\circ\text{C}$), good resistance against chemical attacks and excellent strength at extremely high temperatures [1]. The synthesis of MgAl_2O_4 with specific characteristics such as chemical homogeneity, high purity, low particle size and uniform size distribution depends substantially on preparation methods. As such, magnesium aluminate has been synthesized by various methods such as sol-gel [21,22], solid state [23, 24], spray drying [25], co-precipitation [26], and freeze-drying [27]. However, most of these methods are either complex or expensive which diminishes preparation of the nano-sized materials in a large scale as compared to the combustion or sol-gel synthesis. Moreover, other disadvantages include the necessity of high temperature, inhomogeneity, and low surface area of the nano-sized products. Generally, smaller particle size results in higher surface area which is required for different catalytic applications [28]. Hence, using a hybrid sol-gel combustion method at relatively low temperature is a new and good approach to prepare nanosized magnesium aluminate particles suitable for application in the above-mentioned different fields especially the photocatalytic.

In this study, we report, for the first time, synthesis of MgAl_2O_4 spinel nanoparticles using a hybrid sol-gel combustion method using different fuels such as citric acid, urea, and oxalic acid. The effect of several process parameters on the particle size and morphology of the samples was investigated. The as-prepared products were characterized by FT-IR, XRD, FE-SEM, UV-Vis, and HR-TEM. The photocatalytic degradation of the Reactive Red Me 4 BL dye on the as-prepared product was studied under sun light and illumination of UV radiation.

Experimental

Materials and reagents

All reagents were of analytical grade and they were purchased and used as received without further purification: magnesium nitrate ($\text{Mg}(\text{NO}_3)_2 \cdot 6\text{H}_2\text{O}$; Merck), aluminum nitrate ($\text{Al}(\text{NO}_3)_3 \cdot 9\text{H}_2\text{O}$; Merck), citric acid ($\text{HOC}(\text{COOH})(\text{CH}_2\text{COOH})_2$; Sigma-Aldrich Chemical Co.), oxalic acid ($\text{C}_2\text{H}_2\text{O}_4 \cdot 2\text{H}_2\text{O}$; Sigma-Aldrich Chemical Co.), urea (NH_2CONH_2 ; Fluka) and ammonium hydroxide (25% NH_3 in H_2O ; Sigma-Aldrich Chemical Co.).

One step synthesis of spinel MgAl_2O_4 photocatalyst

A hybrid sol-gel auto combustion method using three different fuels; oxalic acid, urea, and citric acid was used to synthesize magnesium aluminate nanoparticles; A, B, and C samples, respectively. The stoichiometric compositions of the redox mixtures of for the combustion have been calculated based on the total oxidizing (O) and reducing (F) valencies of the oxidizer and fuel so that the equivalence ratio, Φ_c , is unity (i.e. $\Phi_c = (O/F) = 1$), and consequently the energy released by the combustion is maximum for each reaction [29].

In a typical synthesis process: an aqueous solution (30 mL) of magnesium nitrate (4 g, 15.6 mmol) was added to a stirring aqueous solution (50 mL) of aluminum nitrate (11.8 g, 31.2 mmol) to give a Mg/Al molar ratio of 1:2 and the reaction was heated up at $60 \text{ }^\circ\text{C}$, and allowed to stir for 10 min. To the hot stirring solution reaction, urea (5.31 g, 88.5 mmol) dissolved in 50 mL distilled water was added. The reaction solution was heated at $80 \text{ }^\circ\text{C}$ and stirred for 1 h. The produced solution was gelled while heating at $120 \text{ }^\circ\text{C}$. The gel was heated in an electric oven at $200 \text{ }^\circ\text{C}$ for 2 h to give an almost dry and yellowish white mass which was then ignited in an electric furnace at $350 \text{ }^\circ\text{C}$ during which the entire combustion was completed in 10 min. The produced foamy powder was ground and then calcined at various temperatures such as 600 and $800 \text{ }^\circ\text{C}$ for 4 h to give the products referred to as B_{600} and B_{800} , respectively. The produced magnesium aluminate samples (A and C) were prepared by applying similar conditions using oxalic and citric acids fuels, respectively, however, for the C samples pH of the reaction solution was adjusted to pH 5 using ammonium hydroxide aqueous solution (2 M) prior to heating the solution at $80 \text{ }^\circ\text{C}$. Hence, likewise, the subscripts 600 and 800 (for A_{600} , A_{800} , C_{600} , and C_{800}) are referred to the calcination temperatures; 600 and $800 \text{ }^\circ\text{C}$, of the products A and C. The schematic flowchart of the used synthesis process is shown in Scheme 1S.

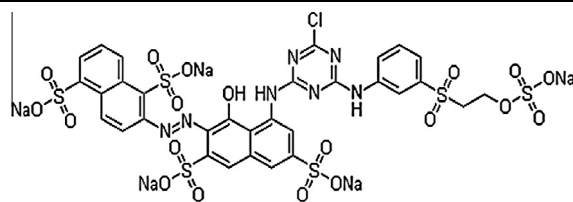
Photocatalytic activity measurements

The photocatalytic degradation of Reactive Red Me 4BL dye (RR4BL) solution by UV light (at 365 nm) and sunlight was investigated using MgAl_2O_4 nanoparticles catalyst (B_{800}) prepared using oxalic acid as fuel. The structure and characteristics of RR4BL dye is given in Table 1. The degradation was investigated in a Pyrex beaker under the UV illumination using a 250 W xenon arc lamp (Thoshiba, SHLS-002) ($\lambda = 365 \text{ nm}$) or under sunlight irradiation by placing the beaker in a sunny place. In each experiment, 0.10 g of catalyst was added to 50 mL of aqueous solution containing 10 mg/L (RR4BL) dye. Prior to illumination, the suspension was magnetically stirred continuously in the dark for 1 h to disperse the catalyst and establish an adsorption/desorption equilibrium. After that, the suspension was irradiated with UV light or Sunlight irradiation. During irradiation process, stirring was continued to keep the mixture in suspension. At given time intervals of irradiation, 3 mL of the dye solution was sampled and centrifugated immediately to remove the MgAl_2O_4 nanoparticles. Then the supernatant solution was analyzed by recording the absorption spectrum of the remained dye using a Jasco UV-Vis spectrophotometer (Jasco; model v530).

Physico-chemical measurements

Powder X-ray diffraction (XRD) of the products was measured using an 18 kW diffractometer (Bruker; model D8 Advance) with monochromated $\text{Cu K}\alpha$ radiation (1) 1.54178 Å). FE-SEM images were recorded using field emission scanning electron microscope (FE-SEM) with a microscope (JEOL JSM-6500F). The HR-TEM images were taken on a transmission electron microscope

Table 1
Structure and characteristics of Reactive Red Me 4BL.

Dye	Reactive Red Me 4BL (RR4BL)
Structure	
Molecular formula	$C_{31}H_{19}ClN_7O_{19}S_6Na_5$
λ_{max}	542 nm
Chemical class	Azo compound
C.I. number	Reactive Red 195

(JEM-2100) at an accelerating voltage of 200 kV by dispersing the samples in ethanol on a copper grid. FT-IR spectra were obtained using FT-IR spectrometer (Bomem; model MB157S) from 4000 to 400 cm^{-1} at room temperature. The optical properties were carried out using a Jasco UV-Vis spectrophotometer (Jasco; model v530).

Results and discussion

Synthesis, morphology and spectral characterization of magnesium aluminate spinel

Fuel effect

A modified sol-gel auto combustion method was used in this work to synthesize $MgAl_2O_4$ nanoparticles based on different kinds of fuels such as urea, oxalic acid and citric acid. The used organic fuels in this investigation played here as a chelating agent and a fuel as well to enhance uniform base conditions that exclude localized precipitation and hence produce a dispersed and wide range of particle size distribution.

In this study the organic materials; urea, oxalic acid and citric acid serve as fuels, in the combustion reaction, oxidized by the nitrate salts; magnesium and aluminum nitrates, to produce $MgAl_2O_4$ nanoparticles. The proposed equations 1–3 for the combustion reactions (Scheme 2S) revealed that the molar ratios of $Mg^{2+}:Al^{3+}$:urea, $Mg^{2+}:Al^{3+}$:oxalic acid, and $Mg^{2+}:Al^{3+}$:citric acid, are 1:2:5.67, 1:2:17, and 1:2:1.89, respectively, corresponds to the situation of an 'equivalent stoichiometric ratio'. In this combustion process, the reaction between the oxidizers (aluminum nitrate and magnesium nitrate) and the fuel is an exothermic reaction which implies that the oxygen content of salt nitrates can be completely reacted to oxidize/consume the used fuel exactly results in enough heat for producing the nanomaterials of interest [15–19]. In addition to producing of the nano-sized $MgAl_2O_4$ product, these reactions give off CO_2 , H_2O , and N_2 gases directly from the reaction between fuel and oxidizer without any need for supplying oxygen from outside. The products were characterized by means of XRD, FT-IR, UV-Vis spectra, FE-SEM and HR-TEM.

XRD study

The phase composition of the synthesized materials was studied using X-ray diffraction analysis. XRD patterns of the magnesium aluminate samples produced by combustion of the dried gel precursors at 600 and 800 °C are shown in Figs. 1 and 2, respectively. It is obvious that the temperature 600 °C was not enough to produce a crystalline product and the product was almost amorphous (Fig. 1). However, on increasing the combustion temperature to 800 °C, crystallinity of the $MgAl_2O_4$ spinel products increased as indicated by the presence of the sharp diffraction peaks in their diffraction patterns in Fig. 2. All the diffraction peaks

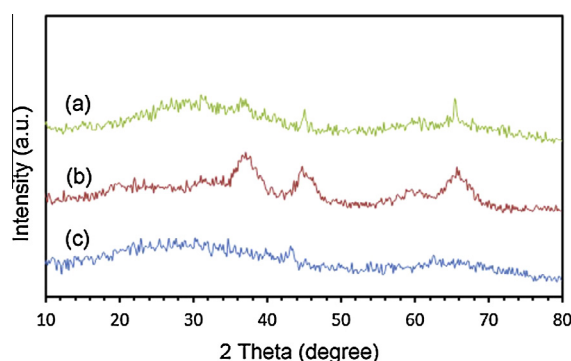


Fig. 1. XRD patterns of $MgAl_2O_4$ samples calcined at 600 °C prepared using oxalic acid (a), urea (b), or citric acid (c) as a fuel.

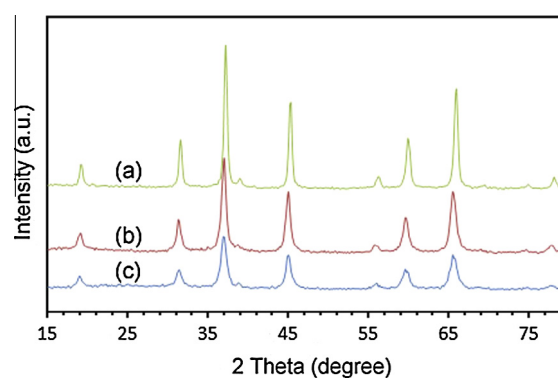


Fig. 2. XRD patterns of $MgAl_2O_4$ samples calcined at 800 °C prepared using oxalic acid (a), urea (b), or citric acid (c) as a fuel.

presented in Fig. 2 can be perfectly indexed to cubic spinel-structured $MgAl_2O_4$. Other peaks of possible intermediate products such as Al_2O_3 and MgO , have not been detected in the patterns which consequently confirm the single phase of the as-prepared $MgAl_2O_4$ nanoparticles. However, the diffraction peaks; curves B and C of Fig. 2, of the $MgAl_2O_4$ nanoparticles product prepared when urea and citric acid, respectively, were used as fuels, could be readily indexed to the cubic spinel $MgAl_2O_4$ with lattice parameters; $a = 8.0788\text{ \AA}$ and $V_{cell} = 527.28\text{ \AA}^3$ (JCPDS File No. 075-1796). On the other hand, when oxalic acid was used as a fuel; curve (a) in Fig. 2, the diffraction peaks of the product were consistent very well with the spinel $MgAl_2O_4$ with cell parameters; $a = 8.010\text{ \AA}$ and $V_{cell} = 513.92\text{ \AA}^3$ (JCPDS File No. 089-1627). Moreover, using the Scherrer equation (1) [30] the crystallite size (D , nm) of the $MgAl_2O_4$ nanoparticles can be evaluated:

$$D = 0.9\lambda / \beta \cos \theta_B \quad (1)$$

where λ is the wavelength of X-ray radiation, β the full width at half maximum (FWHM) of the diffraction peak and θ_B is the Bragg diffraction angle. The estimated average crystallite size of the as-prepared magnesium aluminate nanoparticles was found to be ca. 27.7, 14.6 and 15.65 nm for A_{800} , B_{800} , and C_{800} samples, respectively. Subsequently, it can be easily seen that changing the fuel has a significant effect on the crystallite size of the as-prepared spinel $MgAl_2O_4$ nanoparticles since using the oxalic acid fuel produced the largest crystallite size while the urea fuel produced the finest one.

FT-IR study

The infrared spectra of the as-prepared $MgAl_2O_4$ powders (A_{800} , B_{800} , and C_{800}) annealed 800 °C are shown in Fig. 3 and it seems that the three spectra are almost identical. In the IR spectra, the $MgAl_2O_4$ samples exhibited two characteristic frequencies at ca. 576 and 747 cm^{-1} attributing to the $[AlO_6]$ groups and the lattice vibration of Mg–O stretching, and indicating the formation of $MgAl_2O_4$ spinel samples [31,32]. However, vibration bands around 3515 and 1680 cm^{-1} appeared in the IR spectra of the products could be assigned to the stretching and bending vibrations of the adsorbed surface molecular water interacting with $MgAl_2O_4$ products and the broadness of these bands could be due to hydrogen-bonding O–H [33–37]. The common band at around 2370 cm^{-1} can be accounted to the propagation of the IR beam through air [38].

UV–Vis study

Fig. 4 the UV–Vis spectra of the magnesium aluminate samples (A_{800} – C_{800}) calcined at 800 °C. All samples exhibited two absorption bands which are consistent with the reported data for $MgAl_2O_4$ prepared by another method [39].

However, the band that appeared close to the visible light region for each spectrum may be attributed to the $O^{2-} \rightarrow Al^{3+}$ charge transition due to the excitation of electrons from the valence band of $O(2p)$ to conduction band of $Al(3d)$. Moreover, using the red shifted band, the band gap energy of the synthesized magnesium aluminate can be calculated from the optical absorption edge onset (λ) by the equation [40]: E_g (eV) = 1240/ λ (nm), where λ is the absorption edge and E_g is the band gap energy. The optical band gap energy values were estimated to be 4.13, 4.62 and 4.5 eV for A_{800} , B_{800} and C_{800} magnesium aluminate samples, respectively. From these values, it can be concluded that the energy gap value depends on the crystallite size of the as-prepared

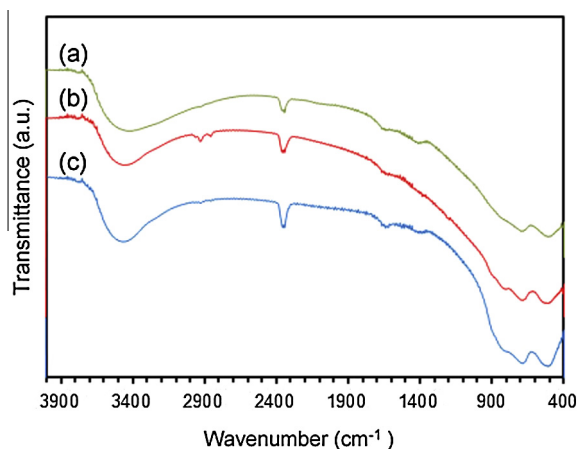


Fig. 3. FT-IR spectra of $MgAl_2O_4$ product calcined at 800 °C prepared using oxalic acid (a), urea (b), or citric acid (c) as a fuel.

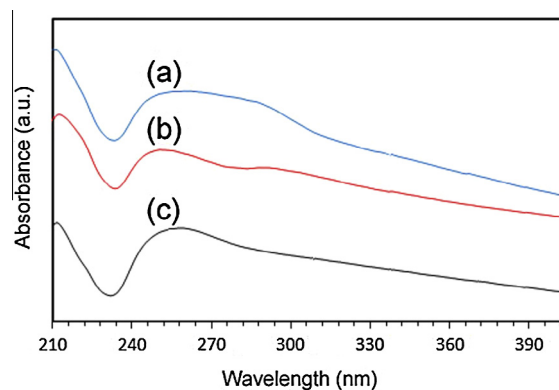


Fig. 4. UV–Vis spectra of $MgAl_2O_4$ product calcined at 800 °C prepared using oxalic acid (a), urea (b), or citric acid (c) as a fuel.

$MgAl_2O_4$ and the largest crystallite size results in the smallest energy gap value and vice versa, which indirectly, means that the fuel has also an influence on the energy gap value.

Morphology study

The particle morphologies of the as-obtained $MgAl_2O_4$ products (A_{800} , B_{800} , and C_{800}) were investigated by field emission scanning electron microscopy (FE-SEM) and presented in Fig. 1S(a–c). A careful inspection of Fig. 1S(a) showed that the product (A_{800}) is actually aggregates of irregular-shaped solid blocks of $MgAl_2O_4$ subcrystals. The average size of these blocks is about 50 μm . On the other hand, Fig. 1S(b and c) revealed that the products (B_{800} and C_{800}) are composed of a layered structure of $MgAl_2O_4$ particles. Moreover, the layers or sheets of the C_{800} product [Fig. 1S(c)] are thinner than that of the B_{800} product. Plus, the aggregates of layers forms in some cases a flower like structures. From this it was concluded that the fuel type in the combustion process could affect the morphology of the product.

For better understanding of the structural and morphological characteristics of the as-synthesized $MgAl_2O_4$ nanoparticles, the products (A_{800} , B_{800} , and C_{800}) have been further examined by high-resolution transmission electron microscopy (HR-TEM), as shown in Fig. 2S(a–c). Fig. 2S(a) revealed that the product A_{800} is composed of dispersed hexagonal and cubic particles with an average diameter of 27.9 nm which is compatible with the crystallite size calculated from the XRD studies. However, on inspection of the micrographs b and c of Fig. 2S(b and c), it can be seen that the products B_{800} , and C_{800} show dense bulk agglomerates, and the particles have both cube like, sphere like, and irregular shapes with an average diameter of 15, and 15.7 nm, respectively, which is consistent well with crystallite size obtained from the XRD studies.

Photocatalytic activity of $MgAl_2O_4$ nanoparticles

The Reactive Red Me 4BL dye degradation over the as-prepared $MgAl_2O_4$ nanoparticles (B_{800} , as a representative example) under UV illumination and under Sun light irradiation was studied to investigate the photocatalytic activity. However, it is worthy to mention that $MgAl_2O_4$ product (B_{800}) prepared using urea fuel has specifically been chosen, in order to exploit high surface area of this product because it has the lowest crystallite size. The UV–Vis spectra of the decomposed RR4BL dye at different reaction times (from 0 to 7 h) under UV illumination and Sun light irradiation were depicted in Fig 5(a and b), respectively. Fig 5(a and b) shows that the dye exhibits an absorption peak at 542 nm and the absorption intensity of the dye solution gradually decreases

in the presence of the as-prepared catalyst with the increase of exposed time, indicating a decrease in the RR4BL dye concentration which consequently means the effective photodegradation of the dye under the magnesium aluminate catalyst. This study revealed that almost 90.0% of the RR4BL dye decomposed under UV illumination within 7 h and, on the other hand, ~95.45% of the dye degraded under sun light irradiation within exposed time 6 h. As shown in Fig. 6(a and b) blank experiments in the absence of the photocatalyst under UV illumination and sunlight irradiation, respectively, show that the photolysis of the dye was negligible. Curves (a) and (b), Fig. 6, show the degree of RR4BL dye degradation in the presence of MgAl_2O_4 nanoparticles as a function of time under UV illumination and sunlight irradiation, respectively. The relative concentration of the dye decreases with the increase of exposed time. However, the adsorption of the dye on the photocatalyst in the dark was also checked as shown in Fig. 6(a and b), and it was found that about 20% of the dye was adsorbed after stirring for 1.0 h and an adsorption/desorption equilibrium was established. The kinetic behavior of the photocatalytic degradation of RR4BL dye was further investigated. It is clear that there is a linear relationship between $\ln(C_a/C_t)$ value and the irradiation time intervals, where C_t is the actual dye concentration at irradiation time t , and C_a is the dye concentration after the adsorption/desorption equilibrium and before the irradiation process. The linear relationships, $\ln(C_a/C_t) = K \times t$, of the curves are presented in Fig. 7, where K is pseudo first order rate constant. Generally, as shown in Fig. 7(a and b), good correlations are obtained indicating that the reaction kinetics follows a pseudo first order rate law and this is the case for both photocatalytic degradation of the dye under UV illumination and sunlight irradiation, respectively. However, the rate constants were estimated to be $5.85 \times 10^{-3} \text{ min}^{-1}$ for photocatalytic degradation of the dye under UV light irradiation and $8.38 \times 10^{-3} \text{ min}^{-1}$ for the photocatalytic degradation under sunlight irradiation. From

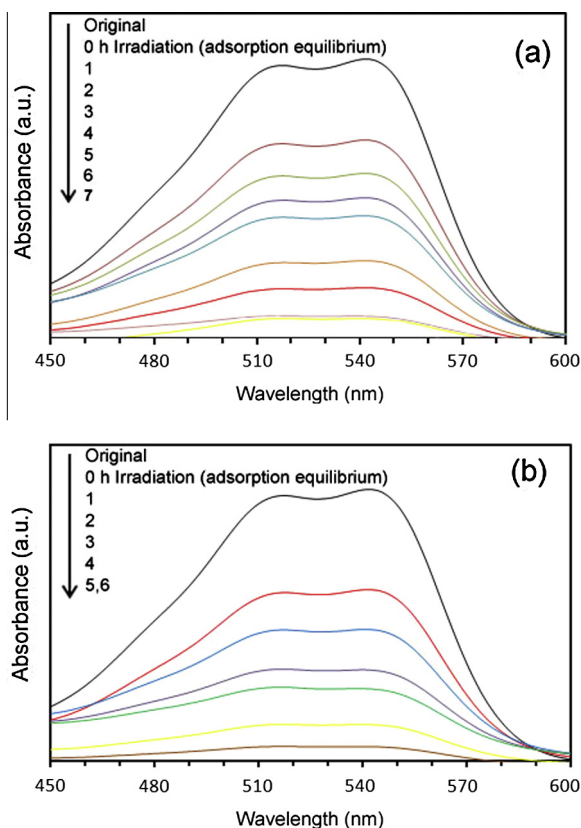


Fig. 5. UV-Vis spectral changes of RR4BL dye solution during the photocatalytic degradation by MgAl_2O_4 (B_{800} sample) under UV (a) or sunlight (b) irradiation.

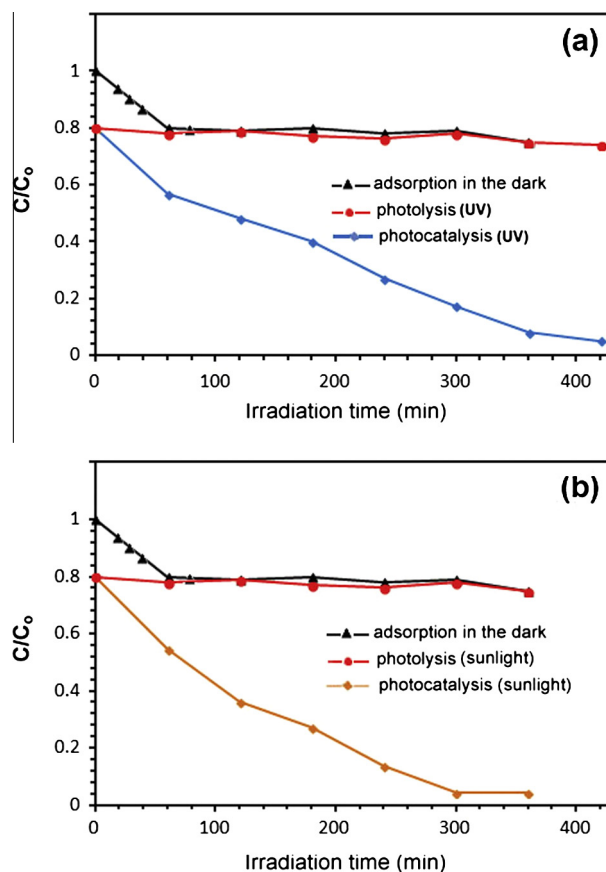


Fig. 6. Photocatalytic degradation of RR4BL dye solution over MgAl_2O_4 (B_{800} sample) under UV (a) or sunlight (b) irradiation.

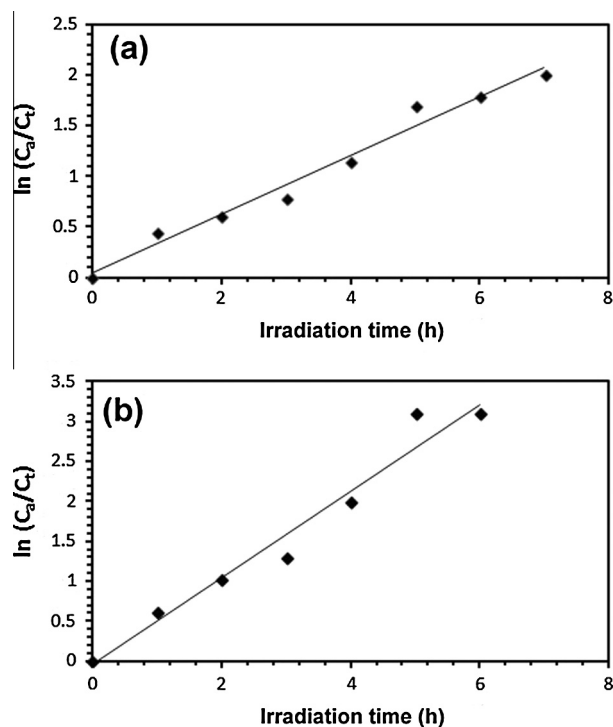


Fig. 7. Reaction kinetics of photocatalytic degradation over MgAl_2O_4 catalyst (B_{800} sample) under UV (a) or sunlight (b) irradiation.

the above results, it can be concluded that the photo-degradation of the RR4BL dye using magnesium aluminate nanoparticles as photocatalyst under sunlight irradiation is more effective and efficient than its photocatalytic degradation under UV light illumination. Scheme 3S presents reactions (1–6) that probably can be proposed to describe the photodegradation of the dye in presence of MgAl_2O_4 catalyst under UV or sunlight irradiation [39–41]. The absorption of light by the catalyst caused transference of an electron from the valence band (VB) to the conduction band (CB) and this process resulted in a hole in the VB and an electron in the CB. The electron–hole pairs, thus generated, can initiate oxidation reduction reactions on the surface of the MgAl_2O_4 particles that are generally responsible for dye degradation. Some of the water molecules ionize according to its dissociation constant into H^+ and OH^- ions. The holes h_{VB}^+ react with the adsorbed OH^- ions to form $^{\bullet}\text{OH}$ radicals (Eqs. (2) and (3)). On the other hand, electrons e_{CB}^- can be trapped by O_2 adsorbed on the surface of the catalyst particles to produce the superoxide radicals (Eq. (4)) which then react with water molecules to give $^{\bullet}\text{OH}$ radicals (Eq. (5)). Subsequently, $^{\bullet}\text{OH}$ and $\text{O}_2^{\bullet-}$ radicals both are responsible and worked together to degrade the RR4BL dye (Eq. (6)). Fig. 3S shows the schematic representation of the proposed mechanism for the photocatalytic degradation of the dye under study.

Conclusion

Pure phase of MgAl_2O_4 nanoparticles can successfully be synthesized by a facile sol–gel auto combustion method using different organic fuels urea, oxalic and citric acid at 250 °C then the burnt product was calcined at 350 °C, separately, for 3.0 h. The prepared sample was characterized by using different tools; FTIR, UV–Vis, XRD, HR–TEM, FE–SEM. The Effect of fuels on the crystallite size of MgAl_2O_3 products was studied. The pure spinel MgAl_2O_4 NPs with average crystallite size 27.7, 14.6 and 15.65 nm was obtained at 800 °C. The produced MgAl_2O_4 NPs showed photocatalytic activity by degradation of 90.0% or 95.45% of the Reactive Red Me 4BL dye under UV or sunlight irradiation, respectively, within ca. 5 h. This degradation process followed pseudo first order law with rate constants of 5.85×10^{-3} and $8.38 \times 10^{-3} \text{ min}^{-1}$ for the aforementioned light respectively.

Appendix A. Supplementary material

Supplementary data associated with this article can be found, in the online version, at <http://dx.doi.org/10.1016/j.saa.2014.04.040>.

References

- [1] B. Ismail, S.T. Hussain, S. Akram, Chem. Eng. J. 219 (2013) 395–402.

- [2] J.S. Piccin, C.S. Gomes, L.A. Feris, M. Gutterres, Chem. Eng. J. 183 (2012) 30–38.
 [3] M.N. Chong, B. Jin, C.W.K. Chow, C. Saint, Water Res. 44 (2010) 2997–3027.
 [4] A.A. Firooz, A.R. Mahjoub, A.A. Khodadadi, M. Movahedi, Chem. Eng. J. 165 (2010) 735–739.
 [5] D.F. Wang, Z.G. Zou, J.H. Ye, Chem. Phys. Lett. 373 (2003) 191–196.
 [6] Z.R. Zhu, X.Y. Li, Q.D. Zhao, H. Li, Y. Shen, G.H. Chen, Chem. Eng. J. 165 (2010) 64–70.
 [7] J.W. Tang, Z.G. Zou, J.H. Ye, Angew. Chem. Int. Ed. 43 (2004) 4463–4466.
 [8] V.B.R. Boppana, D.J. Doren, R.F. Lobo, Chemsuschem 3 (2010) 814–817.
 [9] K. Gurunathan, J.O. Baeg, S.M. Lee, E. Subramanian, S.J. Moon, K.J. Kong, Int. J. Hydrogen Energy 33 (2008) 2646–2652.
 [10] S.W. Cao, Y.J. Zhu, G.F. Cheng, Y.H. Huang, J. Hazard. Mater. 171 (2009) 431–435.
 [11] Y.Y. Jiang, J.G. Li, X.T. Sui, G.L. Ning, C.Y. Wang, X.M. Gu, J. Sol–Gel Sci. Technol. 42 (2007) 41–45.
 [12] D.S. Mathew, R.S. Juang, Chem. Eng. J. 129 (2007) 51–65.
 [13] W.Z. Lv, B. Liu, Q. Qiu, F. Wang, Z.K. Luo, P.X. Zhang, S.H. Wei, J. Alloys Compd. 479 (2009) 480–483.
 [14] Y. Fan, X.B. Lu, Y.W. Ni, H.J. Zhang, M.W. Zhu, Y. Li, J.P. Chen, Appl. Catal. B: Environ. 101 (2011) 606–612.
 [15] D. Kovacheva, H. Gadjev, K. Petrov, S. Mandal, M.G. Lazarraga, L. Pascual, J. Mater. Chem. 12 (2002) 1184–1188.
 [16] A. Saberi, F. Golestani-Fard, H. Sarpooolaky, M. Willert-Porada, T. Gerdes, R. Simon, J. Alloys Compd. 462 (2008) 142–146.
 [17] F.T. Li, Y. Liu, Z.M. Sun, R.H. Liu, C.G. Kou, Y. Zhao, D.S. Zhao, Mater. Lett. 65 (2011) 406–408.
 [18] R. Ianos, I. Lazau, C. Pacurariu, P. Barvinschi, Mater. Res. Bull. 43 (2008) 3408–3415.
 [19] S. Habibzadeh, A. Kazemi-Beydokhti, A.A. Khodadadi, Y. Mortazavi, S. Omanovic, M. Shariat-Niassar, Chem. Eng. J. 156 (2010) 471–478.
 [20] M.J. Iqbal, B. Ismail, C. Rentenberger, H. Ipsen, Mater. Res. Bull. 46 (2011) 2271–2277.
 [21] T. Shiono, K. Shiono, K. Miyamoto, G. Pezzotti, J. Am. Ceram. Soc. 83 (2000) 235–237.
 [22] D. Walker, E.H. Walker Jr., J.W. Owens, M. Etienne, Mater. Lett. 37 (2002) 1041–1050.
 [23] W. Bakkar, J.G. Lindsay, Am. Ceram. Soc. Bull. 46 (1967) 1094–1097.
 [24] L.B. Kong, J. Ma, H. Huang, Mater. Lett. 56 (2002) 238–243.
 [25] Y. Suyama, A. Kato, Ceram. Int. 8 (1982) 17–21.
 [26] R.J. Bratton, Am. Ceram. Soc. Bull. 48 (1969) 759–762.
 [27] C.T. Wang, L.S. Lin, S.J. Yang, J. Am. Ceram. Soc. 75 (1992) 2240.
 [28] P.V.M. Kutty, S. Dasgupta, Ceram Int. 39 (2013) 7891–7894.
 [29] S.R. Jain, K.C. Adiga, V.R.P. Vernekar, Combustion and Flame 40 (1981) 71.
 [30] R. Jenkins, R.L. Snyder, Chemical Analysis: Introduction to X-ray Powder Diffractometry, John Wiley and Sons Inc., New York, 1996.
 [31] S.M. Olhero, I. Ganesh, P.M.C. Torres, J.M.F. Ferreira, Langmuir 24 (2008) 9525–9530.
 [32] J. Puriwat, W. Chaitree, K. Suriye, S. Dokjampa, P. Praserttham, J. Panpranot, Catal. Commun. 12 (2010) 80–85.
 [33] K. Nakamoto, Infrared and Raman Spectra of Inorganic and Coordination Compounds. Part B: Applications in Coordination, Organometallic, and Bioinorganic Chemistry, sixth ed., Wiley-Interscience, USA, 2009.
 [34] M.Y. Nassar, A.S. Attia, K.A. Alfallos, M.F. El-Shahat, Inorg. Chim. Acta 405 (2013) 362–367.
 [35] M.Y. Nassar, Mater. Lett. 94 (2013) 112–115.
 [36] M.Y. Nassar, I.S. Ahmed, Mater. Res. Bull. 47 (2012) 2638–2645.
 [37] M.Y. Nassar, I.S. Ahmed, Polyhedron 30 (2011) 2431–2437.
 [38] M. Huuhtanen, K. Rahkamaa-Tolonen, T. Maunula, R.L. Keiski, Catal. Today 100 (2005) 321–325.
 [39] F.T. Li, Y. Zhao, Y. Liu, Y.J. Hao, R.H. Liu, D.S. Zhao, Chem. Eng. J. 173 (2011) 750–759.
 [40] Q.I. Rahman, M. Ahmad, S.K. Misra, M. Lohani, Mater. Lett. 91 (2013) 170–174.
 [41] H.A. Le, L.T. Linh, S. Chin, J. Jurg, Powder Technol. 225 (2012) 167–175.